molecular pharmaceutics

Article

Biocompatible ELR-Based Polyplexes Coated with MUC1 Specific Aptamers and Targeted for Breast Cancer Gene Therapy

Maria J. Piña, Alessandra Girotti, Mercedes Santos, J. Carlos Rodríguez-Cabello, and F. Javier Arias*

Bioforge Research Group, CIBER-BBN, University of Valladolid, LUCIA, Paseo de Belén 19, 47011 Valladolid, Spain

S Supporting Information

ABSTRACT: The search for new and biocompatible materials with high potential for improvement is a challenge in gene delivery applications. A cell type specific vector made of elastin-like recombinamer (ELR) and aptamers has been specifically designed for the intracellular delivery of therapeutic material for breast cancer therapy. A lysine-enriched ELR was constructed and complexed with plasmid DNA to give positively charged and stable polyplexes. Physical characterization of these polyplexes showed a particle size of around 140 nm and a zeta potential of approximately +40 mV. The incorporation of MUC1-specific aptamers into the polyplexes resulted in a slight decrease in zeta potential but increased cell transfection specificity for MCF-7 breast cancer cells with respect to a MUC1-negative tumor line. After showing the transfection ability of this aptamer-ELR made vector facilitated mainly by macropinocytosis uptake, we demonstrated its application for suicide gene therapy using a plasmid containing the gene of the toxin PAP-S. The strategy developed in this work about using ELR as polymeric vector and aptamers as supplier of specificity to deliver therapeutic material into MUC1-positive breast cancer cells shows promising potential and continues paving the way for ELRs in the biomedical field.

KEYWORDS: ELR, polyplex, aptamer, transfection, breast cancer
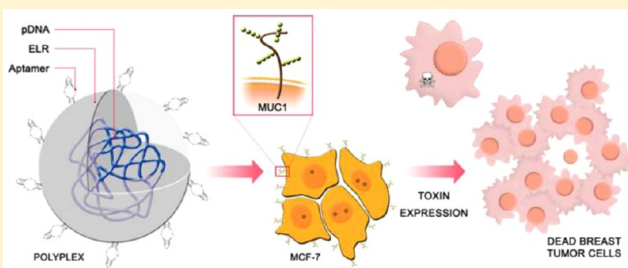
1. INTRODUCTION

Breast cancer is the principal malignancy diagnosed in women in Western societies, with an estimated 230,000 new cases of breast cancer being detected in the female population of the USA during 2014.[1] Although different treatments, namely, surgery, chemotherapy, radiation, endocrine or targeted therapy using Trastuzumab, are available and all of them have been shown to be effective in advanced breast tumors, they improve the clinical outcome but do not increase the cure rate.[2] In the search for alternatives, gene therapy using siRNA, toxic genes, or pro-apoptotic genes, among others, has emerged as one of the most promising strategies for cancer treatment.[3−5] Moreover, the combination of gene therapy with radio- or chemotherapy has shown excellent results.[6−9] One successful approach for gene therapy involves making use of the natural killing ability of toxic agents such as ribosome-inactivating proteins (RIPs). RIPs are RNA N-glycosidases that inactivate by way of a site-specific deadenylation in the large rRNA of eukaryotic and prokaryotic ribosomes.[10,11] Specifically PAP-S (Pokeweed Antiviral Protein from the seeds of *Phytolacca americana*), which is a type I RIP, is a basic monomeric enzyme of approximately 30 kDa lacking a lectin chain.[12,13] Unlike type II RIPs, which are able to penetrate living cells using their cell recognition domain, PAP-S is not cytotoxic. For this reason, it has been used as toxic element in the construction of immunotoxins in different studies.[14−16]

Advanced anticancer therapies require the development of targeted biological strategies in order to maximize efficacy while reducing toxicity. The glycoprotein MUC1 is a membrane-bound glycoprotein containing a variable number of PST domains rich in proline, serine, and threonine, with these residues serving as sites for post-translationally O-linked glycosylation.[17,18] MUC1 is overexpressed in epithelial tumors such as primary and metastatic breast cancer; thus, the O-glycosylation and distribution of this mucin on the cell surface is also known to be altered. Moreover, the overexpression of an under-glycosylated form of MUC1 is reported to have the worst prognosis for breast carcinomas.[19−21] As MUC1 glycoprotein is considered to be a marker for the poor prognosis of breast cancer,[22] it could also be used as a therapeutic target. Increased cell specificity is a constant goal in gene therapy, and in this regard, cell-specific elements such as the short peptide cRGD have been linked to a nonrecombinant polymeric carrier in order to improve the transfection efficiency for vascular diseases.[23] In addition, other targeting agents, including aptamers, have formed a new generation of targeting molecules.[24] Aptamers, which are short (<100 nt of single-stranded DNA or RNA) oligonucleotide sequences, can bind small molecules, proteins, nucleic acids, and even cells and tissues, with high affinity and selectivity.[25] Indeed, aptamers have demonstrated low immunogenicity, good tumor pene-

73 tration, and fast uptake and clearance, thus allowing them to be
74 used to deliver cytotoxic or labeled molecules.[26] There are two
75 interesting aptamers among the list of published MUC1-specific
76 molecules: the S2.2 and 5TR1 (both are 25-base oligonucleo-
77 tide). The aptamer S2.2 binds to the core of MUC1
78 glycoprotein with relatively high affinity and specificity. This
79 aptamer has been studied for diagnostic imaging and
80 radiolabeling in *in vivo* studies.[27,28] In contrast, the aptamer
81 5TR1MUC1 is directed against the underglycosylated PST
82 domains of MUC1 and was previously designed and used for
83 molecular targeting.[29,30]

84   With regard to gene therapy-based strategies, nonviral
85 vectors have been widely studied over the past few years and
86 constitute the most promising alternative for overcoming the
87 immunogenicity problems inherent to viral vectors.[31,32] Thus,
88 complexation of cationic polymers to the genetic material via
89 electrostatic interactions to form polyplexes has been
90 extensively used for gene transfer. PEI (polyethylenimine),
91 PEG (polyethyleneglycol), PLL (poly-L-lysine), chitosan,
92 PLGA (polylactic-coglycolic acid), and PDMAEMA (poly-
93 dimethylaminoethyl methacrylate) are some of the most widely
94 used nonviral gene-delivery vehicles.[33−36] PEI, considered as
95 the gold standard of a polycationic polymer with a high density
96 of amine groups, has been proven to be an efficient nonviral
97 vector due to its ability to bind to the cell surface, its high
98 uptake, and endosomal escape.[37] However, depending on its
99 molecular weight and its branched or linear configuration, this
100 polymer may be toxic.[38]

101   Among other biopolymers, elastin-like recombinamers
102 (ELRs) are protein-based polymers that are becoming
103 increasingly important in different fields of biomedicine.[39−43]
104 The recent development of advanced genetic-engineering
105 techniques allows absolute control over both the architecture
106 of ELRs and their physical and chemical features, especially
107 surface charge, polydispersity, aggregation, and biocompati-
108 bility. ELR chains are randomly extended and under hydro-
109 phobic hydration below the characteristic transition temper-
110 ature (T_t), whereas above this temperature the ELR partially
111 loses its hydration to form an ordered and phase-separated
112 state[44] Nano-, micro- or macro-aggregation phenomena occur
113 above this T_t depending on the architecture and composition of
114 the ELR. Consequently, changing the amino acid composition
115 to include positively charged ones results in ELRs that are more
116 stable at physiological pH and temperature. ELRs have
117 previously been used as oligolysine carriers by the Furgerson
118 group[45] to deliver an EGFP−plasmid inside cells in *in vitro*
119 assays. However, their results showed cytotoxicity effects
120 attributed to the oligolysine. Recently, we have obtained
121 promising results in the use of specifically designed ELRs joined
122 to functional peptides as agents for delivering genes *in vitro*.[46]

123   Cellular transfection can be improved by using positively
124 charged polyplexes that can interact with negatively charged
125 components on the cell membrane, such as proteoglycans and
126 cell-surface receptors.[47,48] Such polyplexes can be internalized
127 by endocytosis and/or direct diffusion processes.[49] Herein,
128 lysine enriched ELR has been specifically design to complex
129 and protect the therapeutic DNA forming stable polyplexes.
130 Moreover, to the best of our knowledge, this is the first time
131 that cancer cell specific aptamers have been incorporated into
132 ELR polyplexes. In this work we reported the design of a
133 specific gene-delivery system for breast cancer based on ELR−
134 pDNA polyplexes with MUC1-specific aptamers adsorbed and
135 applied to suicide therapy using PAP-S expression.

2. MATERIALS AND METHODS

2.1. Chemicals and Cell Lines. pCMVGaussia Luciferase 136
was purchased from Thermo Scientific (USA). The gene of 137
PAP-S[50] was acquired from NZYTECH (Portugal) and 138
inserted into a pCMV plasmid from Clontech (USA). 139
Paraformaldehyde was purchased from Sigma-Aldrich. 140
Twenty-five kDa of branched PEI, polyclonal anti-MUC1 141
antibody, chloroquine, filipin, amiloride, and monodansylcada- 142
verine were purchased from Sigma-Aldrich (Germany). 143
Turbofect and Lipofectamine LTX were purchased from 144
Thermo Scientific (USA). 145

    The aptamers S2.2 (5′GCAGTTGATCCTTTGGATA- 146
CCCTGG′3), 5TR1 (5′GAAGTGAAAATGACAGAACACA- 147
ACA′3) and thiol-modified 5TR1 (5′thiol (C6−S−S)- 148
GAAGTGAAAATGACAGAACACAACA′3) were purchased 149
from Metabion (Germany). Plasmid DNA was prepared 150
using the Endofree Plasmid Giga Kit (Qiagen, Germany). 151

    Normal Human Adipose-Derived Mesenchymal Stem Cells 152
(MSCs, ref R7788−115), basal medium Dulbecco's modified 153
Eagle's medium (DMEM), fetal bovine serum (FBS), 154
penicillin−streptomycin solution, trypsin−EDTA, DPBS, 155
LIVE/DEAD Viability/Cytotoxicity Kit for mammalian cells, 156
and Alamar Blue were supplied by Invitrogen (USA). Human 157
umbilical vein endothelial cells (HUVECs cc-2517) and 158
endothelial growth medium (EGM) were purchased from 159
Lonza (Lonza Walker). Human foreskin fibroblasts (HFF-1, ref 160
SCRC-1041) were purchased from the American Type Culture 161
Collection (ATCC, USA). Human breast cancer (MCF-7, ref 162
86012803) and liver hepatocellular carcinoma (HepG2, ref 163
85011430) cell lines were supplied by Sigma-Aldrich. Eagle's 164
minimum essential medium (EMEM), 2 mM glutamine, and 165
1% NEAA were purchased from Invitrogen. 166

2.2. Synthesis and Characterization of the Cationic 167
ELR. The cationic ELR was created using standard molecular 168
biology techniques and bacterial biosynthesis. This recombi- 169
nant polymer was based on the pentapeptide Val-Pro-Gly-Xaa- 170
Gly (VPGXG) present in elastin, where X is lysine: (VPGKG) 171
×72. The multimeric gene was constructed using the recursive 172
directional ligation method and then inserted into a modified 173
version of pET25b expression vector (Novagen, Germany).[51] 174
The polymer with a controlled length and molecular weight was 175
produced in *Escherichia coli* BLR (DE3) strain (Stratagene, 176
USA) as reported previously.[51] To produce the polymer, the 177
expression vector was transformed into *Escherichia coli* BLR 178
(DE3) strain (Stratagene, USA). Various inverse transition 179
cycles (ITC) were performed to purify the expressed 180
polymer.[51] Endotoxins were removed from the ELR by way 181
of additional NaCl and NaOH treatments.[52] Finally, the 182
polymer was dialyzed against deionized water and freeze-dried. 183
The expected molecular weight and number of amino acids was 184
32 368 Da and 367 amino acids, respectively. 185

    The ELR was characterized by sodium dodecyl sulfate 186
polyacrylamide gel electrophoresis (SDS-PAGE), amino-acid 187
composition analysis, mass spectrometry (MALDI-TOF), 188
proton nuclear magnetic resonance analysis (^{1}H NMR), and 189
dynamic light scattering (DLS). Endotoxin levels were 190
measured using the Endosafe-PTS test (Charles River, USA). 191

    Samples for SDS-PAGE, MALDI-TOF, and DLS were 192
prepared at 1 mg/mL in ultrapure water. For SDS-PAGE, 20 193
μL of solution with 5 μL of loading buffer was loaded on a 194
polyacrylamide gel. For DLS, polymer solution was filtered 195
before measurement using 0.45 μm PVDF syringe filter. 196

For amino acid analysis after addition of a known quantity of α-aminobutyric acid as internal pattern, the polymer sample was hydrolyzed (6 M HCl, 1% phenol, and 2.5 h at 155 °C) and evaporated. The powder was resuspended in 1 mL of 20 mM HCl and a 1/10 dissolution was prepared. The quantification of the less represented amino acids was made from the most concentrated sample and the quantification of the most represented amino acids from the 1/10 dissolution.

For ^{1}H NMR, 10 mg of polymer was solved in 600 μL of $(CD_3)_2SO$.

2.3. Preparation and Nomenclature of ELR Complexes. To prepare the polyplexes, the ELR was dissolved in ultrapure water to a concentration of 1 mg/mL, and they were left at 4 °C overnight. Complexes were formed in aqueous solution by mixing the pDNA with the ELR solution in the appropriate N/P ratios, where N corresponds to the number of amine groups from the polymer and P to the phosphate groups from the plasmid DNA. The mixtures were vortexed at 25 °C for 1 min and incubated at 25 °C for 30 min for nanocomplex formation. For experiments involving polyplexes and aptamers, a solution of each aptamer (S2.2 or 5TR1) in ultrapure water was added to the ELR/pDNA polyplex and the mixture left for a further 30 min at room temperature. The complexes were formed and designated according to the different N/P/P*apt* ratios, where P*apt* corresponds to the number of phosphate groups in the aptamers, maintaining the N/P ratio constant and increasing P*apt* by adding more aptamer.

2.3.1. Formation of ELR−Aptamer Polyplexes Conjugated with Au Nanoparticles. ELR polyplexes were formed as described in section 2.3 at a 50/1/4 N/P/P*apt* ratio, although in this case the 5′-thiol-modified 5TR1 aptamer was complexed with the polyplex and incubated for 30 min at room temperature. Gold nanoparticles (Sigma-Aldrich, USA) were mixed with the polyplex solution to a final concentration of 5 nM and incubated for 5 min at room temperature.

2.4. Physical Characterization of ELR−pDNA Polyplexes. *2.4.1. Calculation of T_t for the ELR in the Presence of pDNA.* ELR−pDNA complexes were formed at three different N/P ratios (5/1, 10/1, and 50/1). After complexation, the pH was adjusted with NaOH 1 M or HCl 1 M, and dynamic light scattering (DLS) measurements (Zetasizer NanoZs from Malvern Instruments Ltd., UK) were performed at pH 5.0, 7.5, and 11.5 in the temperature range 30−65 °C in order to calculate the corresponding T_t.

2.4.2. Gel Retardation Assay and pDNA Protection. The ELR−pDNA complexes were prepared at different N/P ratios (0.5, 1, 2, 3, 5, and 10/1). For the DNA protection experiment, polyplexes and pDNA were additionally treated with the restriction enzyme *Dpn* I (Thermo Scientific, USA) for 90 min. All preparations were loaded onto a 0.8% agarose gel, and electrophoresis was carried out in 1× TAE buffer at 60 mV for 120 min, staining with SimplySafe (EURx, Poland). The complexed pDNA was visualized by exposure to UV light in a transilluminator (Vilber, Germany).

2.4.3. Particle Size and Zeta Potential. The particle size and zeta potential of the ELR/pDNA/aptamers at different ratios were measured using the Zetasizer NanoZs at a temperature of 37 °C. Z-average mean (nm) and zeta potential (mV) were used for data analysis. Experiments were repeated three times.

2.4.4. Transmission Electron Microscopy (TEM). TEM measurements were performed using a JEOL JEM-1230 electron microscope operating at 120 kV. The polyplex solution was dropped onto carbon-coated copper grids and images recorded after drying for 4 h at 37 °C.

2.5. Cell Culture. Human breast cancer (MCF-7) and liver hepatocellular carcinoma (HepG2) cell lines were maintained in EMEM supplemented with 10% FBS, 2 mM glutamine, 1% NEAA, and antibiotics (culture media) at 5% CO_2 and 37 °C. Human mesenchymal stem cells (hMSC) and human fibroblasts (HFF-1) were cultured in DMEM supplemented with 100 U·mL^{-1} penicillin, 0.1 mg·mL^{-1} streptomycin, and 10% or 15% FBS, respectively. Human umbilical vein endothelial cells (HUVEC) were grown in complete endothelial growth medium. Cells were incubated at 37 °C under 5% CO_2, and their medium was replaced every 2 days.

2.6. Transfection Assays. *2.6.1. Effect of Polyplex− Aptamer System on Cell Viability.* MCF-7 and HepG2 cells were plated at 3×10^4 cells per cm^2 and incubated overnight. Afterward, both cell lines were incubated with the ELR−pDNA polyplexes formed with 0.5 μg of pCMV-Gaussia Luciferase plasmid at different ratios and 1 μg pf PEI, used as reference polymer, under the same conditions for 5 h in FBS-free culture medium. After this time, the medium was replaced with a medium supplemented with 10% FBS and the cells incubated for a further 43 h at 37 °C.

The relative number of metabolically active cells was evaluated using the Alamar Blue assay according to the manufacturer's guidelines. Thus, the culture was incubated in 10% Alamar Blue solution in minimum medium for 4 h at 37 °C and under a 5% CO_2 atmosphere. Subsequently, 80 μL of the reduced medium was transferred to a 96-well plate. Untreated cells were considered to represent 100% viability. The fluorescence intensity of test samples and controls was measured at an emission wavelength of 590 nm after excitation at 560 nm using a SpectraMax M2 microplate reader (Molecular Devices, USA).

2.6.2. Analysis of Transfection Efficiency by Luciferase Expression. A total of 3×10^4 cells per cm^2 of MCF-7 or HepG2 was seeded onto 96-well plates and grown at 37 °C, 5% CO_2 overnight. Cells were incubated in a serum-free medium for 5 h in the presence of the polyplexes (ELR: pCMV Gaussia luciferase) at specific N/P ratios with gradually increasing P*apt* ratio for both S2.2 and 5TR1 aptamers. The medium was then replaced by fresh serum-containing medium, and the cells cultured for a further 43 h. One microgram of PEI and 3 μL of Lipofectamine LTX or 1 μL of Turbofect to complex the pDNA were used as positive control. Additional transfection experiments with the cells preincubated with 50:1 anti-MUC1 for 1 h at 37 °C, and experiments with incubation of polyplexes in the presence of 10% of serum enriched medium for 5 h, replaced by a fresh one, and cultured for a total of 48 h were accomplished. At this point a 20 μL aliquot was removed from the culture medium and mixed with the luciferase substrate (Thermo Scientific, USA). The light produced was measured using a SpectraMax L luminometer (Molecular Devices, USA). The protein content of the lysate was determined by a Bradford assay using a microplate reader. Luciferase expression is given as relative light units (RLU) per milligram of total protein.

2.6.3. Cell Uptake Assays. 2.6.3.1. Polyplex Internalization Measured by Flow Cytometry. MCF-7 was seeded at 3×10^5 cells per well onto six-well plates and left to grow at 37 °C, 5% CO_2 overnight. Subsequently, cells were incubated with the polyplexes containing fluorescein-labeled pCMVGaussia luciferase (purified using LabelIT Tracker, Mirus Bio LLC, USA) and the 5TR1 aptamer (N/P/P*apt* 50:1:4) in serum-free

medium for 3 h. After this time the medium was replaced, and cells were harvested with 0.05% trypsin−EDTA, washed with D-PBS 1×, twice, fixed with 4% paraformaldehyde and washed again with D-PBS 1×. Flow cytometry analysis was performed to assess the fluorescein internalized in cells (Gallios flow cytometer. Beckman-Coulter).

2.6.3.2. Polyplex Uptake Visualized by Fluorescence. The same protocol from 2.6.3.1 section was followed and an additional treatment with trypan blue was performed for the Z-series in order to visualize the internalized labeled polyplexes. Samples for confocal, phase-contrast, epifluorescence, and differential interference contrast (DIC) microscopy were fixed in 4% paraformaldehyde for 10 min. Internalization of the polyplex−aptamer into cells was analyzed using a Leica SP5 confocal microscope (Leica Microsystems, Heidelberg). Z-series were performed with a Z-step of 0.45 μm. Fluorescein fluorophore and phase-contrast images were overlaid to obtain a multilayer image using ImageJ (provided by NIH, version 1.47v).

Bright-field and fluorescence microscopy were performed using a NIKON Eclipse Ti fluorescence microscope equipped with a digital camera system (Digital sight DS-2MBWc) (Nikon, Japan).

Additionally, counterstaining of nucleus with 300 nM of DAPI was performed, and a z-stack composed by four images with a z focal difference of 0.2 μm was performed. Further orthogonal projection of z−y planes showing the pDNA nuclear collocation was accomplished.

2.6.4. Assessment of Internalization Pathway. The same protocol as 2.6.2. Section was applied for MCF-7 cells pretreated with 25 μM of chloroquine, 1 μg mL^{-1} of filipin, 5 μg mL^{-1} of amiloride, and 100 μM of monodansylcadaverine in media without serum. After inhibitors treatment, media was replaced by fresh ones containing polyplexes.

2.6.5. Assays of Cell Transfection by PAP Expression. MCF-7, HepG2, MSC, HUVEC, and HFF-1 cells were seeded onto 96-well plates in a quantity of 3×10^4 cells per cm^2 for tumor cells and 1×10^4 cells per cm^2 for primary cells, in order to maintain the same levels of confluence for all the cell lines and allowed to grow at 37 °C, 5% CO$_2$ overnight prior to polyplex treatment.

For these experiments, the polyplexes ELR−pDNA (N/P 50/1) and ELR−pDNA−aptamer (N/P/Papt 50/1/4) were formed using the pCMV-PAP plasmid. Cells were incubated with the nanocomplexes at 37 °C, 5% CO$_2$ for 5 h. After this time, the medium was replaced with fresh medium containing 10% FBS, and the cells incubated at 37 °C, 5% CO$_2$ for a further 43 h. Cell death was quantified using the LIVE/DEAD assay following the manufacturer's instructions and measured at an emission wavelength of 620 nm after excitation at 525 nm using a SpectraMax M2 microplate reader (Molecular Devices, USA).

2.7. Statistical Analysis. The RLU/mg in transfection of ELR−pDNA polyplexes was analyzed using Student's *t* test. All results with $p < 0.05$ for three independent experiments were considered to be statistically significant.

3. RESULTS

3.1. Synthesis and Characterization of the Cationic ELR. The obtained ELR gene corresponding with the amino acid sequence MESLLP (VPGKG)$_{72}$V where the pentapeptide VPGKG is repeated 72 times, was corroborated by gene sequencing. The main property of this polymer is its high number of lysine amino acids, which confer it a positive charge, together with its temperature- and pH-responsive behavior. The efficiency of the ELR production process was assessed by several physical and chemical techniques; SDS-PAGE, amino-acid composition analysis, MALDI-TOF, ^{1}H NMR (Figure S1). The overall results displayed a high purity polymer with suitable chemical compositions (Figure S1). The amino-acid analysis showed an appropriate composition, and the differences can be attributed to the experimental error of the technique. As reflected in the MALDI-TOF spectrum, the experimental molecular weight of the ELR was 32 314.1 Da (SD: ±1.7), whereas the expected value was 32 368 Da. Additionally, the production yield of the bioprocess was 90 mg/L cell culture and the final endotoxin levels were less than 10 EU/mg, which is adequate for *in vitro* transfection assays.[52,53] In addition, the T_t of the ELR was assessed by DLS at different pH values. Thus, T_t for the ELR at 10.5 μM in aqueous solution was above 60 °C for all the pH tested.

3.2. Physical Characterization of ELR−pDNA Polyplexes. The ability of the ELR to complex pDNA was previously confirmed by electrophoresis mobility of DNA, where the pDNA was fully retained from the N/P ratio of 2/1 (Figure S2A). Additionally, the stability of the complex in the presence of endonuclease restriction enzyme was probed confirming the ability of ELR to protect the plasmid DNA (Figure S2B).

3.2.1. Transition Temperature for the ELR in the Presence of pDNA. Since a change of 50% in the scattering intensity is considered as the transition temperature,[54] the T_t of ELR in aqueous solution was found to be close to 60−70 °C for pH 11.5 (Figure S3).

When ELR was complexed with pDNA, and polyplexes were kept at physiological conditions of pH (5−7) and temperature (37 °C), the complexes remained stable at all the N/P ratios tested (Figure S3). However, when the pH was increased to 11.5, the presence of pDNA decreased this T_t as can be appreciated for 50/1 ratio polyplexes (Figure 1). An increase in pH led to a decrease in T_t, with a striking variation in light scattering at pH 11.5 for all N/P ratios tested. The destabilization of polyplexes upon increasing the pH to 11.5
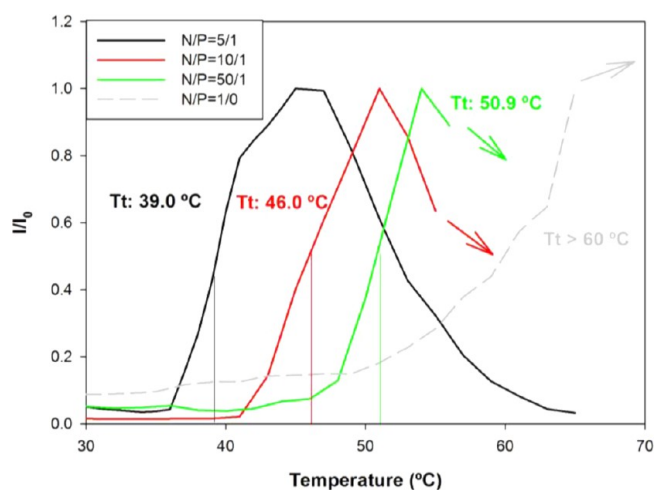
Figure 1. Normalized scattered light intensity as a function of temperature at pH 11.5 for ELR−pDNA polyplexes at different N/P ratios. Arrows indicate the decreasing trend in light scattering as a result of the presence of microaggregates with increasing temperature.
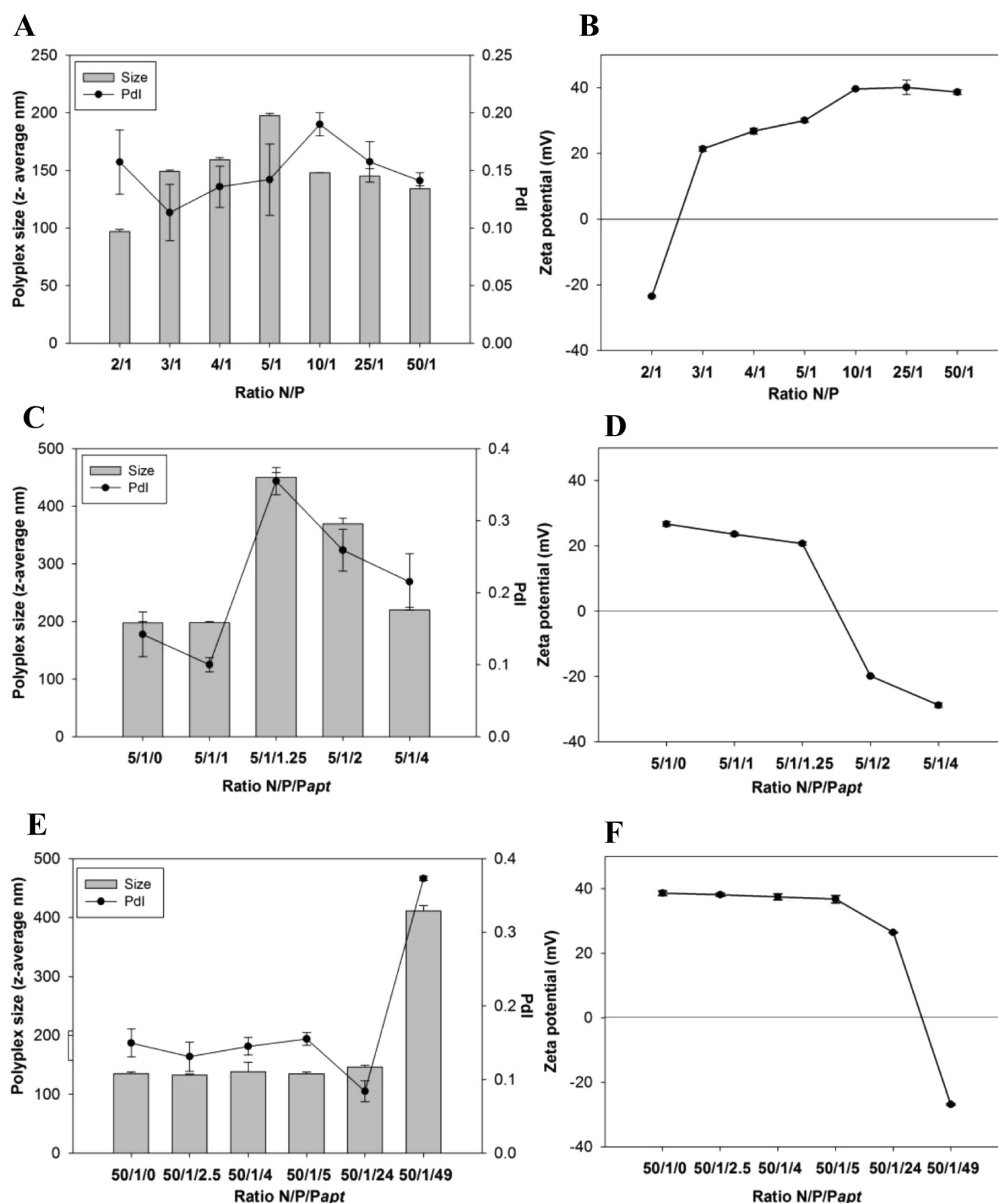
Figure 2. Size, polydispersity index (PdI), and zeta potential for the ELR–pDNA polyplexes. Size (A) and zeta potential (B) for ELR–pDNA polyplexes with an N/P ratio ranging from 2/1 to 50/1. Size (C) and zeta potential (D) for ELR–pDNA–aptamer complexes with an N/P/Papt ratio ranging from 5/1/0 to 5/1/4. Size (E) and zeta potential (F) for ELR–pDNA–aptamer complexes with an N/P/Papt ratio ranging from 50/1/0 to 50/1/49 ($n = 3$, mean ± SD).

became more evident in the decrease in normalized light scattering to around 0.1 for all N/P ratios at lower temperatures and by the presence of two size-distribution groups. One of these groups corresponds to the free ELR, with a size of around 10−20 nm, and the other to the ELR polyplex, with a size of around 100−200 nm (Figure S4). Additionally, nano- and microaggregation process between polyplexes occurred. Furthermore, an increase in the N/P ratio from 5/1 to 50/1 also resulted in an increase in T_t (Figure 1). Consequently, herein we provide evidence that the ELR–pDNA polyplexes are stable complexes at physiological conditions in all the ratios tested, and they are not influenced by the smart behavior inherent to ELRs, which is present at the highest pH.

3.2.2. Particle Size and Zeta Potential. The size of these ELR–pDNA complexes was determined by DLS (Figure 2) and found to range from about 100 nm at an N/P ratio of 2/1 to 200 nm at an N/P ratio of 5/1, with a polydispersity index (PdI) ranging from 0.11 to 0.20 (Figure 2A). The progressive increase in size and polydispersity observed was found to be correlated with an increase in the zeta potential up to an N/P ratio of 5/1. At an N/P ratio of 10/1, and despite having the highest PdI, the size decreased. From ratios of 10/1 to 50/1, the size and zeta potential remained constant at about 140 nm and +40 mV, respectively (Figure 2A,B). Both 5/1 (size of about 200 nm) and 50/1 (size of about 140 nm) ratios with a similar zeta potential but different size, were chosen to assess the effect of addition of the aptamer 5TR1 on polyplex size and stability by adding increasing amounts of aptamer (Papt) once the polyplexes had formed. A similar concentration-dependent effect was observed at both ratios, with polyplex size increasing with aptamer ratio up to a value at which charge-neutralization occurred (50/1/49 or even earlier at 5/1/2; Figure 2E,C). Similarly, there was a striking increase in PdI at the N/P/Papt
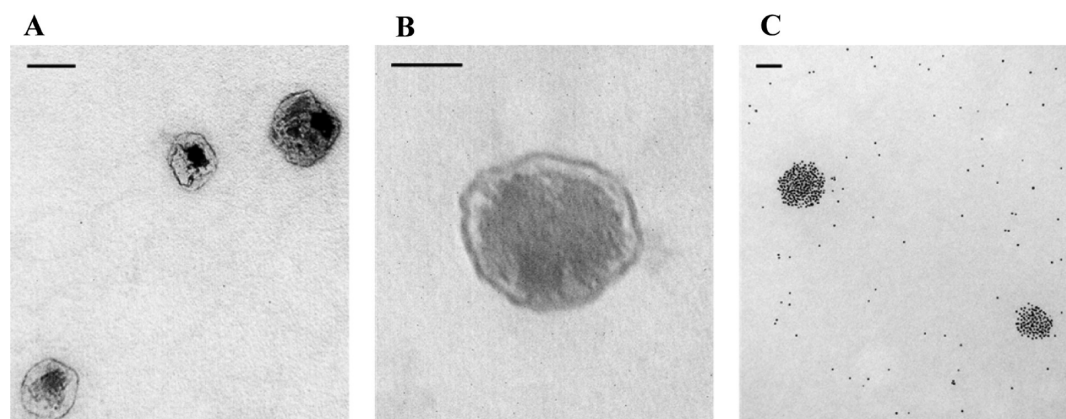
Figure 3. Transmission electronic microscopy images showing the morphology and shape of polyplexes in aqueous solution. ELR−pDNA polyplexes at a 50/1 N/P ratio (A). ELR−pDNA−aptamer polyplexes at a 50/1/4 N/P/Papt ratio with aptamer 5TR1 (B). ELR−pDNA−aptamer polyplexes at a 50/1/4 N/P/Papt ratio with thiol-modified aptamer 5TR1 and gold nanoparticles (C). Scale bars correspond to 100 nm in A and C and 50 nm in B.

ratio corresponding to the highest size for ratios of both 5/1 and 50/1.

Additionally, a further study of polyplex surface charge was performed using the zeta potential. The results of this study showed a progressive increase in zeta potential from −23 mV (N/P 2/1) to nearly +40 mV (N/P 10/1), with the value being dependent on polymer concentration (Figure 2B). At N/P ratio of 2/1 the polyplex exposes the negative charges from the plasmid outward. At this low ratio, the positive charge from the amine groups in the ELR seems to be strongly affected by the presence of phosphate groups from the pDNA and the hydrophobic environment derived from the ELR polymer structure. A striking increase from negative to positive values was observed on going from a ratio of 2/1 to 3/1, and stabilization of the surface charge was observed from 10/1 to 50/1 ratio. However, the addition of higher aptamer concentrations initially resulted in a slight decrease in the zeta potential at the low N/P ratio of 5/1, with a marked drop being observed at 5/1/2 (Figure 2D). In contrast, the behavior of the high ratio polyplex (50/1) showed the formation of a stable positively charged particle (+40 mV) up to a ratio 50/1/24, with a striking drop for the neutralization ratio 50/1/49 (Figure 2F).

3.2.3. Microscopic Analysis of Polyplexes Morphology. The morphology of the polyplex was further characterized by TEM at a ratio of 50/1 in the absence (Figure 3A) and presence (Figure 3B,C) of aptamer 5TR1 adsorbed on the polyplex at an N/P/Papt ratio of 50/1/4. As can be seen from these figures, the 50/1 polyplexes possess a rounded shape with a size (123.8 nm ± 12.1 SD) that correlates with the values obtained by DLS (134.1 nm ± 2.5 SD). The pDNA appears to be located inside the polyplex with the polymer surrounding it, as can be seen from the different density of the particle nucleus (Figure 3A). Additionally, there appears to be no difference in the morphology of these two kinds of polyplexes (Figure 3A,B). A further study that showed the noncovalent absorption of the aptamer to the polyplex surface was performed. To this end, gold nanoparticles (5 nm) were mixed to a polyplex previously made with a thiol-modified 5TR1 aptamer. The resulting complexes (Figure 3C) possess a homogeneous shape and a size in agreement with the TEM (Figure 3B) and DLS values (Figure 2E), indicating that the gold nanoparticles mainly cover the surface of the polyplexes where the thiolated aptamer should be present.

3.3. Transfection Assays. In light of the previous studies, cell viability and transfection experiments were performed in order to assess the suitability of the polyplex complexes for breast cancer gene therapy. The human cell lines used for the transfection assays were two tumoral cell types, namely, MCF-7, which is a breast cancer line overexpressing the MUC1 glycoprotein[55] as cell model for gene therapy, and HepG2, a hepatocarcinoma cell line with no MUC1 expression.[56] Given the physical characterization results for the ELR−pDNA polyplexes discussed above, N/P ratios of 5/1 and 50/1 were chosen to test transfection in these human cell lines. At a 5/1 ratio the polyplex has a size of about 200 nm and a zeta potential of about +30 mV, whereas at a 50/1 ratio the nanoparticle has a size of around 150 nm and a zeta potential of almost +40 mV, which confers more stability on the complex and should therefore increase the transfection efficiency.

3.3.1. Effect of the Polyplex−Aptamer System on Cell Viability. As a requisite for gene therapy applications, we evaluated the cytotoxicity of ELR−pDNA polyplexes formed with the innocuous pCMV-Gaussia Luciferase plasmid DNA at different N/P/Papt ratios along with the aptamers S2.2 and 5TR1 in MCF-7 and HepG2 cell lines. Since the viability levels at ratio of 5/1/0 were essentially 100%, only the effect of the ratio with higher amounts of polymer and increasing quantities of aptamer is shown (Figure 4). No polyplex-induced cytotoxicity was observed for any of the cell lines from a ratio of 50/1/0 to 50/1/49, whereas the value of cell viability reached nearly 150% in the breast cancer line when a higher proportion of aptamers was used. The viability of cells incubated with ELR polyplexes was compared with PEI polyplexes formed with the same innocuous plasmid but without aptamers. In our experiments, this polymer exhibited marked cytotoxicity in MCF-7 cells, for which the viability decreased to about 20%, in contrast to the results shown by ELR polyplexes.

3.3.2. Luciferase Expression. Once the lack of toxicity from the ELR−pDNA−aptamer complexes had been confirmed, it was necessary to assess their suitability as nonviral gene carriers with cancer cell line specificity conferred by the MUC1 aptamers (5TR1 and S2.2) by using the pDNA encoding for a luciferase enzyme. To this end, MCF-7 (MUC1+) and HepG2
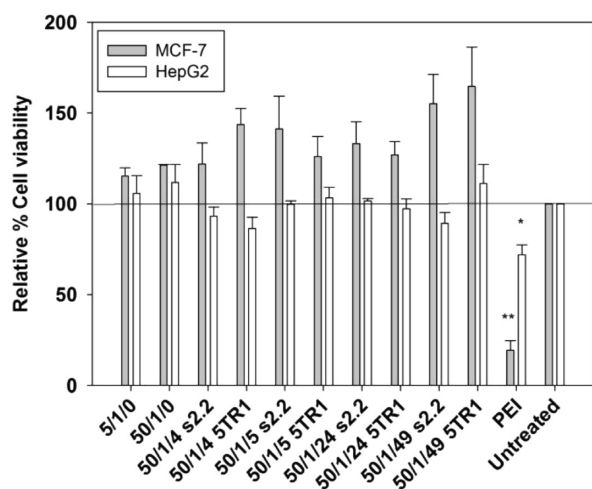
Figure 4. Viability of MCF-7 and HepG2 cell lines at different N/P/Papt ELR−pDNA ratios for aptamers S2.2 and 5TR1. Cells were coincubated with the polyplexes, and a viability assay was performed for all samples. Untreated cells were considered as 100% viability control and PEI polyplexes as a reference transfection system ($n = 3$ independent experiments, mean ± SD). *$p < 0.05$, **$p < 0.01$.

(MUC1-) cells were transfected with ELR−pDNA polyplexes with both N/P ratios and including the aptamers.

The effect of both types of polyplexes was first studied using MUC1+ cells in order to determine the best candidate. As shown in Figure 5A, there were important differences in luciferase expression in MCF-7 cells between the two ELR polyplexes. Thus, in the absence of aptamers, the 50/1 polyplex was found to be more efficient than the 5/1 ratio, exhibiting a 10-fold higher luciferase expression. However, the most marked differences were observed after incorporation of the aptamers. Thus, the use of different ratios of the two aptamers with the 5/1 polyplex had little effect on MCF-7 transfection, whereas the incorporation of both oligonucleotides into the 50/1 polyplex produced an aptamer-dependent amplification of its transfection efficiency. Five different aptamer concentrations were used in the test, and in both cases, higher aptamer concentrations resulted in lower transfection. At low ratios

(N/P/Papt 50/1/4) the transfection efficiency increased at least 6-fold with respect to the nude polyplexes. However, transfection was also annulled when the aptamers neutralized their charge (50/1/49), as can be seen from Figure 2E,F. As regards the effect of each aptamer, clear differences were also seen when used with the 50/1 polyplex. Thus, in the positively charged polyplexes (50/1/4 to 50/1/24), the aptamer 5TR1 was found to be significantly more efficient for MCF-7 transfection than S2.2, with a maximum increase of 2.5-fold. This feature was dramatically affected when the aptamer concentration neutralized the polyplexes (50/1/49 ratio), thereby annulling the MUC1 specificity of the aptamers.

In light of these results, the 50/1 polyplex was chosen for the remaining experiments concerning the transfection effect in several human cell lines. In an initial study, the specificity induced by the presence of MUC1 in cancer lines was studied using the HepG2 hepatocarcinoma cell line lacking MUC1 expression. As can be seen from Figure 5B, significant differences in luciferase expression ($p < 0.001$) were found between both cell lines at this ratio, which was higher for the MUC1 overexpressing MCF-7 cells irrespective of the aptamer used. Since the best results of transfection were obtained for 50/1/4 using 5TR1 aptamer, following studies will be focused on this condition. Blockade of MUC1 was performed by the pretreatment of cells with anti-MUC1 antibody for 1 h at 37 °C (Figure S5). After that time, transfection with 50/1/0 and 50/1/4 polyplexes was performed. The result showed a total inhibition of 5TR1 specificity in which the transfection levels of 50/1/4 lowered up to 50/1/0 levels. By contrast, 50/1/0 transfection was not affected by the presence of the antibody, which support the evidence of the interaction between 5TR1 and MUC1. In addition commercially available agents like PEI, Lipofectamine, or Turbofect were tested, and comparable levels of transfection were found for MCF-7 cells (Figure S6), being the transfection for ELR−pDNA−aptamer polyplexes at 50/1/4 ratio slightly higher than Turbofect and in the same order (1×10^8 RLU mg^{-1} protein) than PEI. Further studies of transfection in the presence of 10% of serum were accomplished (Figure S7) as well. A reduction of gene expression was found for both ELR without (2.7 times) and with aptamer (1.6 times). The highest decrease corresponded
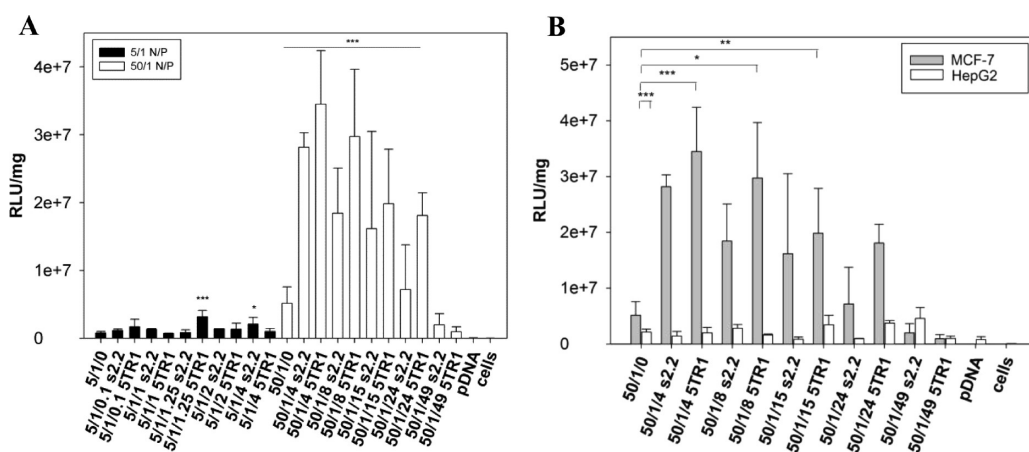
Figure 5. Luciferase expression by pCMV-Gaussia Luciferase contained in ELR−pDNA−aptamer polyplexes. (A) Polyplexes at a 5/1 N/P ratio with different Papt ratios for aptamers S2.2 and 5TR1 in MCF-7 cells. (B) Polyplexes at a 50/1 N/P ratio with different Papt ratios for aptamers S2.2 and 5TR1 in MCF-7 and HepG2 cells. Luciferase activity is expressed in RLU/mg protein lysate. The polyplex without aptamers and pDNA were used as controls. The results are expressed in logarithmic scale as mean ± standard error of three independent experiments. *$p < 0.05$, **$p < 0.01$, ***$p < 0.001$.
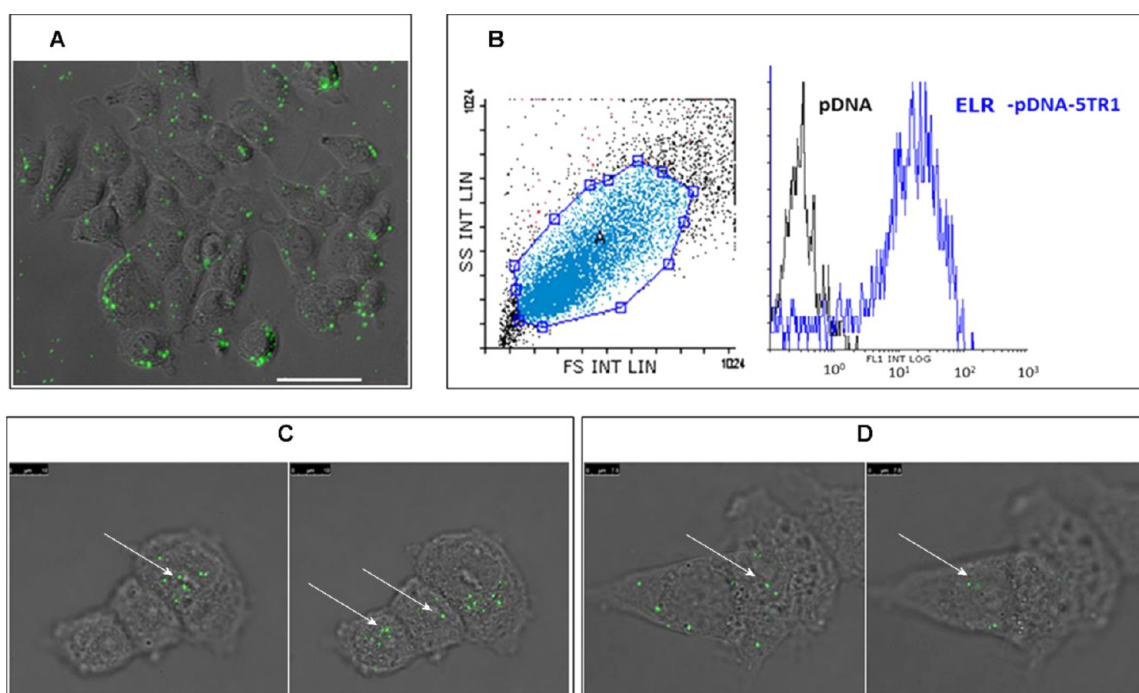
Figure 6. Cellular uptake of ELR−pDNA−5TR1 polyplexes with fluorescein-labeled pDNA. (A) Fluorescence microscopy image of MCF-7 treated with ELR−pDNA−5TR1 nanoparticles for 3 h (merged image of the phase-contrast and FITC channels). The scale bar corresponds to 50 μm. (B) Flow cytometry analysis of MCF-7 cells incubated with polyplexes. Gate A, which corresponds to FITC+ cells, was set on the side-scatter vs forward-scatter histogram. The cell count was plotted as a function of FL1, which corresponded to the FITC channel for pDNA and ELR−pDNA−5TR1 transfected cells. (C,D) Confocal microscopy images of MCF-7 containing fluorescein-labeled polyplexes. Merged bright- and fluorescence-field images of different focal planes have been analyzed. The nuclear areas of cells with the bright green dots of polyplexes are indicated by arrows. Cells from C and D were treated with trypan blue in order to discriminate fluorescent polyplexes inside the cell. Scale bars correspond to 10 μm.

for the polyplex alone showing the retention of the specificity by the system ELR−pDNA−aptamer in the presence of serum.

3.3.3. Cellular Uptake of Polyplexes. The intracellular uptake of these ELR−pDNA−5TR1 polyplexes was confirmed using various techniques. To this end, MCF-7 cells were incubated with 50/1/4 polyplexes containing fluorescein-labeled pCMV-Gaussia Luciferase plasmid for 3 h, and the resulting internalization process was initially visualized by fluorescence microscopy (Figure 6A). Although a few polyplexes were observed on the surface of the tissue culture plaque, a broad distribution of nanoparticles associated with the cells could also be seen. The labeled cells were then detached with trypsin, in order to remove the external binding fluorescence signal that could interfere with the detection of the intracellular polyplexes,[57,58] washed with PBS and analyzed by flow cytometry. The results were compared with cells transfected using the fluorescent plasmid alone (Figure 6B). The data showed a marked internalization of polyplexes of 85.76 ± 12.35% (mean ± SD) for all cells, in comparison with cells treated with fluorescein-labeled pDNA alone (1.70 ± 1.68%). Finally, trypan blue treated cells were visualized by confocal microscopy in a z-series succession explained in Figure S8 where the two focal planes confirmed the presence of polyplexes inside the cells (Figure 6C,D) and the likely presence of fluorescent plasmid inside the nucleus (indicated by arrows). An additional visualization with the nucleus stained with DAPI evidenced the presence of pDNA inside the nucleus (Figure S9).

This group of assays demonstrated the cellular internalization and nuclear localization of ELR−pDNA polyplexes equipped with cell specificity provided by the MUC1-directed aptamers.

3.3.4. Assessment of the Internalization Pathway. Once the uptake of ELR−pDNA−5TR1 polyplexes was visualized, the investigation of the relation between the internalization pathway and subsequent gene expression was accomplished. MCF-7 cells were treated with a variety of endocytosis inhibitors for 30 min at 37 °C and incubated with polyplexes for 5 h at 37 °C. After this time, polyplexes were removed, cells were incubated up to 48 h and luciferase activity was measured. Inhibition of Na^+/H^+ exchange required for macropinocytosis by means of amiloride decreased the luciferase expression to 26% after transfection with ELR−pDNA−5TR1 polyplexes. Moreover, inhibition of caveolae-mediated endocytosis by filipin decreased the expression to 44%, and inhibition of clathrin mediated endocytosis by dansylcadaverine resulted to inhibit the expression to 60%. Additionally, the inhibition of acidification in acidic vesicles by chloroquine did not affect significantly the luciferase expression. This data showed evidence about the primary influence of macropinocytosis and in a lesser extent of caveoline and clathrin-endocytosis pathways over the gene expression (Figure 7).

3.3.5. Effect of Toxin Transfection on Human Breast Cancer Cells. Since we have previously shown that ELR polyplexes are able to reach the nucleus and express their genetic material in a specific manner, now polyplexes with the construct pCMV-PAP as pDNA and surrounded by 5TR1 aptamer at a 50/1/4 ratio (5 μg pDNA mL^{-1}) were used to transfect five different human cell lines, namely, the tumor cell lines MCF-7 (MUC1+) and HepG2 (MUC1−) and three human primary cell types (fibroblasts (HFF-1), endothelial (HUVEC), and mesenchymal stem cells (MSC)), to assay the effects of polyplexes on their viability.
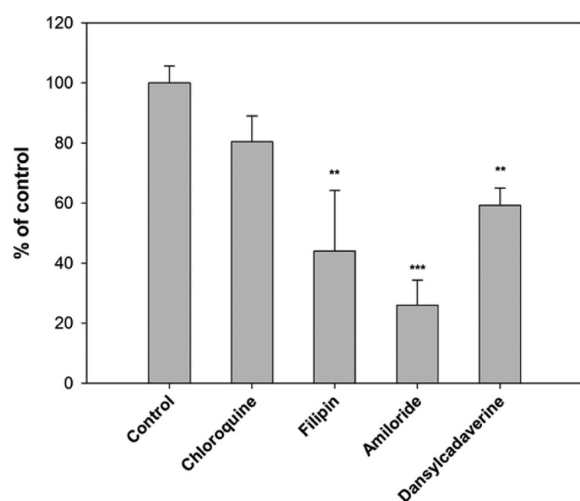
Figure 7. Luciferase expression of ELR−pDNA−5TR1 polyplexes at 50/1/4 ratio in the presence of different inhibitors in MCF-7 cells. Polyplexes were incubated with cells after treatment with 25 μM of chloroquine, 1 μg/mL of filipin, 5 μg/mL of amiloride, and 100 μM of monodansylcadaverine. The results expressed as % of control are mean ± standard error of three independent experiments. *p < 0.05, **p < 0.01.

The viability of the five cell lines subjected to the different treatments was shown by fluorescence (Figure 8). Cells acquired their typical morphology in all cases. The endothelial, mesenchymal, and fibroblast cell cultures appeared to have the lowest cell death (Figure 8, MSC, HUVEC, and HFF1 columns). By contrast, the human liver (Figure 8, HepG2 column) and breast (Figure 8, MCF-7 column) cancer cell lines were both affected by coincubation with the ELR/pCMV-PAP polyplex containing aptamer or not. However, a higher number of dead cells was found for MCF-7 in comparison with the MUC1-HepG2, and an improved cytotoxic effect was visualized for MCF-7 cells treated with the polyplex 5TR1.

In order to quantify the results observed by fluorescence microscopy, the effect of PAP-S expression was quantified in terms of percentage of dead cells in both HepG2 and MCF-7 tumor cells (Figure 9). ELR−PAP−5TR1 polyplexes were found to efficiently kill MUC1+ breast cancer cells with a 95% of death rate after incubation for 48 h. The incorporation of 5TR1 aptamer at the surface of the ELR−PAP polyplexes resulted in a significant increase of nearly 25% in dead MCF-7 cells. In contrast, no differences in percentage of dead cells for polyplexes with aptamer (33%) and polyplexes alone (40%) were found for the tumoral (MUC1−) HepG2 cells. Additionally, no significant differences were observed between any of the polyplex−aptamer conditions tested in human primary cells (HUVEC, MSC, and HFF-1) with levels of cell death similar to those for untreated cells. These results highlight the selective effect of the transfected plasmid in breast cancer cells presenting MUC1 in comparison with other tumor and primary cells.

4. DISCUSSION

A variety of strategies have been applied in order to design biomaterials with application in gene therapy. Herein we report the design of a specific gene-delivery system for breast cancer based on ELR−pDNA polyplexes and complexed with MUC1-specific aptamers. The ELR used in this study was constructed using recombinant techniques, thus giving them a high level of

versatility and allowing the incorporation of positively charged amino acids, such as lysine in a simple manner. The main property of this ELR is its high number of lysines, which are responsible for its temperature- and pH-responsive behavior at physiological conditions.

In order to verify that the designed ELR based polyplexes were stable despite of the ELR smart temperature-responsive behavior, an initial study analyzing the effect of different conditions of pH and temperature over the T_t was conducted. Most of the polymers used for transfection are positively charged, thus allowing them to complex with the negatively charged pDNA. Considering the T_t as an intrinsic characteristic of ELRs, this results in a double effect for the polymer, namely, an electrostatic interaction between the polymer and pDNA via the lysines, which leads to polyplex formation, and the smart behavior of the ELR, which triggers its aggregation and conformational change above T_t. This T_t can be changed by extrinsic factors such as the addition of negatively charged phosphate groups. For these ELR based polyplexes, it was possible to observe variation in the T_t only at pH 11.5. Thus, the presence of negatively charged phosphates due to incorporation of the pDNA into the ELR triggered polyplex formation and, consequently, a change in the polarity of the polymer, decreasing the T_t at pH 11.5 (Figure 1). Additionally, the variation in pH and N/P ratio showed marked effects on the T_t. Thus, a decrease in T_t occurred for all ratios when the pH was increased at pH 11.5 (Figure S3). The free ε-amino groups from the L-lysines (pKa 10.5) in the polyplex are largely deprotonated at this pH, thereby decreasing the net polarity of the complex and promoting destabilization of the polyplexes. The lower light scattering at lower temperatures and the presence of free ELR corroborated this process (Figure S4). Two consecutive effects, namely, initial incorporation of free ELR to the polyplex and a consecutive drop in the scattered intensity as a result of a cooperative increase in the hydrophobicity of the polymer and aggregation into micron- and nanoscale particles between the ELR on the outside of the polyplexes, were perceived upon increasing the temperature at pH 11.5 (Figure 1). Similarly, an increase in T_t was observed upon increasing the amount of polymer. It is remarkable to highlight that polyplexes at physiological pH of 7.5 and 5 are stable due to the absence of transition by the ELR, which make them useful for gene delivery applications (Figure S3).

Besides the requirement of stable polyplexes, an appropriate particle size is necessary to obtain positive results in cell transfection. Particles with a size of about 200 nm are known to be internalized by endocytosis.[59,60] The polyplexes obtained ranged from 100 to 200 nm, which is appropriate for cellular uptake. A progressive increase in size, polydispersity, and zeta potential was found up to a 5/1 ratio when increasing the N/P ratio. From 10/1 to 50/1 significant constant values were observed, thereby suggesting a higher stability of the polyplex compared with the previous ratios (Figure 2A,B). The influence of addition of the aptamer 5TR1 was evaluated with 5/1 and 50/1 polyplex ratios: the result was a concentration-dependent effect. Additionally, a 50/1 ratio produced more stable polyplexes than 5/1 ratio due to the increase in polydispersity and charge neutralization at higher ratios (50/1/49). The gradual incorporation of aptamer provided more negatively charged phosphates to interact with, and neutralize, the free ε-amino groups from L-lysines, thereby affecting the charge and stability of the polyplex. In contrast the presence of aptamers did not affect the shape or size of the particles (with exception

Figure 8. Representative fluorescence microscopy images for MSC, HUVEC, HFF1, MCF-7, and HepG2 cells after 5 h of coincubation with minimum medium (untreated), pDNA, ELR−pDNA (polyplex), and ELR−pDNA conjugated with 5TR1 aptamer (polyplex 5TR1) where the pDNA contained PAP-S transgene under the CMV promoter. The coincubation was followed by 48 h of incubation under standard culture conditions.

of 50/1/49 ratio), which is in accordance with the DLS results (Figures 2E and 3A,B). The surface charge density studied as zeta potential is directly related to the stability of many colloidal systems, and it is thought that a positive zeta potential should favor interaction with the cell membrane.[48] However, the incorporation of aptamers that provide cell specificity may decrease the surface charge of the polyplex. This hypothesis was corroborated in the assays conducted in this work. Initially, the location of the polymer on the periphery of the polyplex where it exposes its positively charged ε-amino groups to the exterior while maintaining a neutralized charge inside was shown from N/P ratio of 3/1. The subsequent incorporation of increasing amounts of aptamer resulted in a marked decrease in the surface charge of the ELR−pDNA due to neutralization of the system and a widespread distribution of the aptamers on the

polyplex surface, with polyplexes at a 50/1 ratio being more stable than those at a 5/1 ratio. The decrease in the surface charge density of polyplexes at higher concentrations of aptamer suggests the location of these aptamers on the polyplex surface. By contrast, at lower ratios of aptamer the surface charge density of the polyplex is highly positive pointing the location of amino groups from polymer outward. The outside arrangement of amino groups favors the interaction of aptamers with the polyplex surface. Additionally, the presence of aptamers in the polyplex was supported by the visualization of gold nanoparticles bound to thiol-containing aptamers (Figure 3C) what are thought to be located on the polyplex surface despite of this technique does not allow to confirm this distribution, and some may be also entrapped. The polyplexes obtained in this work represent an improvement with regard to
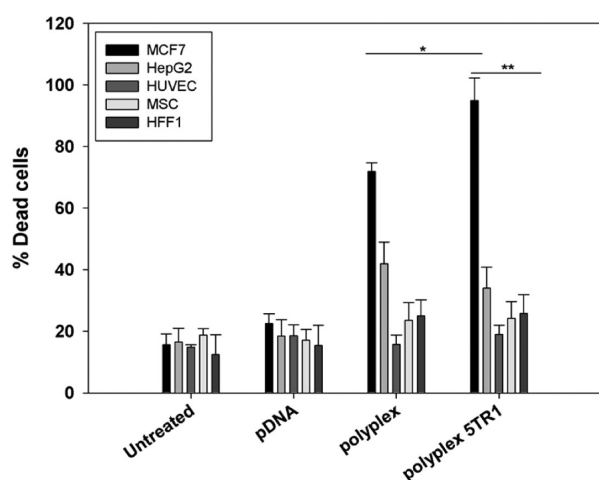
Figure 9. Targeted killing ability of ELR–PAP–5TR1 polyplexes. Percent dead cells was calculated by fluorescence quantification. Cells were preincubated for 5 h with minimum medium (untreated), pCMV-PAP plasmid alone (pDNA), ELR–pDNA (polyplex), and ELR–pDNA conjugated with aptamer 5TR1 (polyplex 5TR1). Additional incubation under standard conditions up to 48 h was then carried out. Mean ± standard error of three independent experiments. A statistical analysis showed significant differences (*$p <$ 0.05, **$p <$ 0.01).

previous studies[46] concerning the zeta potential and stability of particles besides the incorporation of breast cancer cell specific aptamers.

ELRs as naturally inspired recombinant polymers are characterized by their biocompatibility in terms of lack of cytotoxicity and immunogenicity. This has been assessed in both *in vitro* and *in vivo* assays thus making them appropriate for local and systemic administration.[52,61] Similar results were obtained in *in vitro* studies involving positively charged ELRs.[41] In light of these findings and the physical characterization of the polyplexes, their cytotoxicity with S2.2 and 5TR1 aptamers was evaluated using both cancer lines. The results showed that the cell viability of MCF-7 cells incubated in the presence of polyplexes with different ratios was clearly higher than 100% and about 100% for HepG2 (Figure 4). A similar increase in viability was previously observed in a murine myoblastoma cell line,[62] human breast cancer cell line,[63] and mesenchymal stem cells,[64,65] when treated with several ELRs and, recently, when C6 rat glioma cells were coincubated with ELR polyplexes,[46] thereby demonstrating the friendly nature of these recombinant polymers as well as the supplemental specificity conferred by the aptamers on MUC1+ cells. In contrast, a high level of cytotoxicity was found for cells treated with PEI, probably due to the presence of free PEI after formation of polyplexes, which disrupts the plasmatic membrane and causes necrosis.[66,67] Although PEI is commonly used in transfection for *in vitro* assays, it often has a strong cytotoxic effect, depending on the cell line, as reported elsewhere.[66,68] Nowadays research is focusing in decreasing this toxicity by the use of biocompatible molecules such as chitosan or employing PEG as shell.[69,70] In contrast, previous studies with positively charged ELRs incubated with blood components showed the innocuous character of these polymers[46] making them useful for intravenous administration.

The next step was the evaluation of transfection level and cell specificity provided by the MUC1 aptamers. Since the binding specificity of both aptamers had been previously studied for MCF-7 cells[29,71] we focused on evaluating the improvement provided by the aptamers with respect to the ELR–pDNA system. Figure 5 shows the marked improvement in transfection when using a 50/1 ratio, thus indicating that the physical characteristics of the nanoparticles (150 nm and +40 mV in 50/1 versus 200 nm and +27 mV in 5/1) have a clear influence on transfection efficiency. The most striking differences were found when aptamers were incorporated, also being higher for a 50/1 ratio. An aptamer-dependent amplification of transfection was observed for 50/1 ratio, with the lower 50/1/4 ratio being the best of those ratios tested with comparable transfection levels to PEI and no toxic effects. In contrast, the transfection values achieved in the presence of aptamers were lower when the latter were used in excess. This indicates that the positive effect of aptamers is blocked, probably, according to the physical results (Figure 2C,D), due to the formation of unstable and inefficient nanoparticles in which increasing quantities of aptamers produce, first bigger and more polydisperse polyplexes and second negatively charged surfaces. These effects over the transfection levels together with potential zeta values and TEM reinforce the hypothesis of polyplexes coated with MUC1 aptamers. Differences were also found between both aptamers, with the 5TR1, which targets the underglycosylated PST domains of MUC1, being more efficient than S2.2, which targets the MUC1 core. In light of these results, the 50/1 ratio was chosen for the remaining transfection experiments with MCF-7 and HepG2 cell lines (Figure 5B). Initially, the specificity of the polyplex–aptamer system was evaluated using the MUC1-HepG2, with significant differences in luciferase expression being found between both cell lines. These differences were higher for the MUC1 overexpressing MCF-7 cells irrespective of the aptamer used. Consequently, the intracellular uptake of ELR–pDNA– aptamer polyplexes is MUC1-dependent and is more efficient when a rational quantity of the 5TR1 aptamer is used. The influence of serum in transfection was also evaluated, and showed a reduction for the polyplex with and without aptamer (Figure S7). By contrast, this reduction was higher for the polyplex alone; this circumstance can be explained by the general reduction in transfection activity in polymeric polyplexes. Other commercially available systems such as PEI possess a decrease in transfection when serum is present in several cell lines such as fibroblasts and BMSCs.[72] However, it is remarkable to note that the specificity of the system ELR– pDNA–aptamer was retained despite of the presence of serum. This situation points the possibility of using this system for local or even systemic administration.

The uptake of ELR–pDNA–5TR1 polyplexes by the targeted breast cancer cells was visualized by fluorescence microscopy and quantified by flow cytometry. The results showed marked internalization of the polyplexes with cytoplasmic and even nuclear location of pDNA in MUC1 overexpressing MCF-7 cells (Figure 6 and S9). Consequently, the overall results allow us to establish the basis for their use as a plasmid carrier in gene therapy in a safe and specific manner.

The internalization pathway was assessed by the effect of different inhibitors over the luciferase expression. As shown in Figure 7 the higher inhibitory effect was observed when cells were pretreated with amiloride, which inhibit the Na^+/H^+ exchange required for macropinocytosis. It suggests the primary uptake of ELR–pDNA–5TR1 polyplexes by this macropinocytosis pathway. In the same manner, polyplexes appeared to be internalized in a lower proportion by caveolin and

890 clathrin-dependent endocytosis. In fact MUC1 glycoprotein
891 uptake by macropinocytosis and clathrin-dependent pathways
892 has been previously reported,[18,29] which evidence the
893 interaction of 5TR1 aptamer with the MUC1 located on the
894 cell surface. Further study with chloroquine was performed in
895 order to evaluate the effect of the inhibition of endosome-
896 lysosome maturation over the gene expression. Chloroquine
897 basifies the acidic vesicles and accumulates in them; this fact did
898 not involve a significant decrease in luciferase expression.
899 Herein we can suggest the independence on acidic pH for
900 ELR−pDNA−5TR1 polyplexes endosomal escape. We hy-
901 pothesize that their interaction with MUC1 would somehow
902 favor the escape from endosome since it is known the existence
903 of high levels of MUC1-C in cytoplasm and even the nuclear
904 presence of both MUC1-C and MUC1-N.[73,74]

905 Since one of the major challenges in gene therapy is to use
906 the natural killer ability of cytotoxic agents or cell death
907 inducers to selectively eliminate undesirable cells,[75] the
908 expression of a ribosome inactivating protein was studied in
909 this work. As described previously, PAP-S has a potent
910 cytotoxic activity but only once it reaches the cytoplasm of
911 the cell. Hence, when the plasmid containing PAP-S gene is
912 delivered inside of cells by the ELR device and expressed by the
913 cell machinery it should be able to permanently disable the
914 ribosomes by arresting the function of elongation factors EF-1
915 and EF-2 thereby causing cell death.[12] Since we used a plasmid
916 codifying the PAP-S toxin and bearing in mind their potential
917 use for in vivo therapy, the transfection effect of ELR−PAP−
918 5TR1 polyplexes was tested in five different human cell lines
919 including nontumoral primary cells. The tumoral cell lines
920 MCF-7 (MUC1+) and HepG2 (MUC1−) and three human
921 primary cell types (HFF-1, HUVEC, and MSC) were chosen.
922 Fibroblasts were selected as the most representative cell type of
923 connective tissue.[76] MSCs are pluripotent cells that have been
924 reported to have both stimulatory and suppressive effects in
925 breast cancer.[77] HUVEC allowed us to study the influence of
926 our transfection system in a model of endothelial function due
927 to the likely intravenous application of gene therapy treatments.
928 As shown in Figure 7, incubation of cells with the different
929 treatments did not affect the cell morphology for any of the
930 lines. Additionally, MCF-7 and HepG2 tumor cells were the
931 only ones clearly affected by the presence of the polyplex.
932 Similarly, there was a remarkably higher sensitivity of MCF-7
933 cells to PAP-S in comparison with other nonoverexpressing
934 MUC1 cell lines. A significant increase in the percentage of
935 death in breast cancer cells was found reaching nearly 95%
936 (Figure 9) when the 5TR1 aptamer was incorporated into the
937 polyplex thereby suggesting an efficient expression of functional
938 PAP-S in the transfected cells. However, no increase was
939 observed between polyplex and polyplex−5TR1 treatment for
940 MUC1-HepG2 cells. Indeed, the lowest cytotoxic effects were
941 observed when primary cells were incubated with polyplexes.
942 The fact that the effects observed were similar to those for
943 untreated cells suggests a possible protective effect on them. It
944 is interesting to note that the limited effect on MSCs,
945 endothelial and fibroblasts under conditions in which tumor
946 cells have been shown to be extensively affected, is remarkable
947 as it allows us to hypothesize that either local or systemic
948 intravenous route of administration could be used without
949 damage to the bloodstream lineage. These results corroborate
950 the suitability of ELR−5TR1 aptamers for a specific suicide
951 therapy with a novel use of PAP-S as transfecting agent
952 affecting only target breast cancer cells.

5. CONCLUSION

953 In summary, we have developed a nonviral gene-delivery
954 system comprising tailor-made elastin-like recombinamers and
955 MUC1 aptamers with potential application in the treatment of
956 breast cancer. When bound to plasmid DNA, this polymer is
957 able to self-assemble and form a polyplex stable at physiological
958 conditions and possesses a positively charged surface, a suitable
959 particle size for cell internalization, and cell line specificity
960 provided by the aptamers. This system selectively delivers
961 plasmids bearing luciferase and PAP-S genes into tumor cells
962 while protecting normal human cells. Accordingly, the use of
963 this ELR−aptamer system is a promising strategy in the
964 delivery of therapeutic genes of interest that target breast tumor
965 cells even more considering the high potential of ELRs for
966 improvement. Therefore, further research focusing on in vivo
967 experiments will be conducted.

■ ASSOCIATED CONTENT

968

ⓢ Supporting Information

969
970 The Supporting Information is available free of charge on the
971 ACS Publications website at DOI: 10.1021/acs.molpharma-
972 ceut.5b00712.

973 Characterization of the ELR by MALDI-TOF, NMR,
974 SDS-PAGE, and amino-acid analysis; assays performed to
975 determine the influence of pDNA, temperature, and pH
976 on the ELR−pDNA polyplexes in terms of condensation
977 ability, transition temperature (T_t), particle size, and
978 DNA protection; transfection assays and a scheme for z-
979 series and z-stack figures (PDF)

■ AUTHOR INFORMATION

980

Corresponding Author
981
982 *E-mail: arias@bioforge.uva.es.

■ ACKNOWLEDGMENTS

989

■ REFERENCES

1002

1003 (1) American Cancer Society.. Cancer Facts and Figures 2014, 1−63.
1004 (2) Gonzalez-Angulo, A. M.; Morales-Vasquez, F.; Hortobagyi, G. N.
1005 Overview of resistance to systemic therapy in patients with breast
1006 cancer. Adv. Exp. Med. Biol. 2007, 608, 1−22.
1007 (3) Filleur, S.; Courtin, A.; Ait-Si-Ali, S.; Guglielmi, J.; Merle, C.;
1008 Harel-Bellan, A.; Clezardin, P.; Cabon, F. SiRNA-mediated inhibition
1009 of vascular endothelial growth factor severely limits tumor resistance to

antiangiogenic thrombospondin-1 and slows tumor vascularization and growth. *Cancer Res.* **2003**, *63* (14), 3919–22.

(4) Garg, H.; Salcedo, R.; Trinchieri, G.; Blumenthal, R. Improved nonviral cancer suicide gene therapy using survivin promoter-driven mutant Bax. *Cancer Gene Ther.* **2010**, *17* (3), 155–63.

(5) Li, Y.; Li, L. J.; Wang, L. J.; Zhang, Z.; Gao, N.; Liang, C. Y.; Huang, Y. D.; Han, B. Selective intra-arterial infusion of rAd-p53 with chemotherapy for advanced oral cancer: a randomized clinical trial. *BMC Med.* **2014**, *12*, 16.

(6) Wang, H.; Nan, L.; Yu, D.; Agrawal, S.; Zhang, R. Antisense anti-MDM2 oligonucleotides as a novel therapeutic approach to human breast cancer: in vitro and in vivo activities and mechanisms. *Clin. Cancer Res.* **2001**, *7* (11), 3613–24.

(7) Ciardiello, F.; Caputo, R.; Troiani, T.; Borriello, G.; Kandimalla, E. R.; Agrawal, S.; Mendelsohn, J.; Bianco, A. R.; Tortora, G. Antisense oligonucleotides targeting the epidermal growth factor receptor inhibit proliferation, induce apoptosis, and cooperate with cytotoxic drugs in human cancer cell lines. *Int. J. Cancer* **2001**, *93* (2), 172–8.

(8) Vlachaki, M. T.; Chhikara, M.; Aguilar, L.; Zhu, X.; Chiu, K. J.; Woo, S.; Teh, B. S.; Thompson, T. C.; Butler, E. B.; Aguilar-Cordova, E. Enhanced therapeutic effect of multiple injections of HSV-TK + GCV gene therapy in combination with ionizing radiation in a mouse mammary tumor model. *Int. J. Radiat. Oncol., Biol., Phys.* **2001**, *51* (4), 1008–17.

(9) Shim, G.; Han, S. E.; Yu, Y. H.; Lee, S.; Lee, H. Y.; Kim, K.; Kwon, I. C.; Park, T. G.; Kim, Y. B.; Choi, Y. S.; Kim, C. W.; Oh, Y. K. Trilysinoyl oleylamide-based cationic liposomes for systemic co-delivery of siRNA and an anticancer drug. *J. Controlled Release* **2011**, *155* (1), 60–6.

(10) Nielsen, K.; Boston, R. S. RIBOSOME-INACTIVATING PROTEINS: A Plant Perspective. *Annu. Rev. Plant Physiol. Plant Mol. Biol.* **2001**, *52*, 785–816.

(11) Girbes, T.; Ferreras, J. M.; Arias, F. J.; Stirpe, F. Description, distribution, activity and phylogenetic relationship of ribosome-inactivating proteins in plants, fungi and bacteria. *Mini-Rev. Med. Chem.* **2004**, *4* (5), 461–76.

(12) Barbieri, L.; Battelli, M. G.; Stirpe, F. Ribosome-inactivating proteins from plants. *Biochim. Biophys. Acta, Rev. Biomembr.* **1993**, *1154* (3–4), 237–82.

(13) Stirpe, F.; Battelli, M. G. Ribosome-inactivating proteins: progress and problems. *Cell. Mol. Life Sci.* **2006**, *63* (16), 1850–66.

(14) Kreitman, R. J. Immunotoxins for targeted cancer therapy. *AAPS J.* **2006**, *8* (3), E532–51.

(15) Yang, W. H.; Wieczorck, M.; Allen, M. C.; Nett, T. M. Cytotoxic activity of gonadotropin-releasing hormone (GnRH)-pokeweed antiviral protein conjugates in cell lines expressing GnRH receptors. *Endocrinology* **2003**, *144* (4), 1456–63.

(16) Erice, A.; Balfour, H. H., Jr.; Myers, D. E.; Leske, V. L.; Sannerud, K. J.; Kuebelbeck, V.; Irvin, J. D.; Uckun, F. M. Anti-human immunodeficiency virus type 1 activity of an anti-CD4 immunoconjugate containing pokeweed antiviral protein. *Antimicrob. Agents Chemother.* **1993**, *37* (4), 835–8.

(17) Burchell, J. M.; Mungul, A.; Taylor-Papadimitriou, J. O-linked glycosylation in the mammary gland: changes that occur during malignancy. *J. Mammary Gland Biol. Neoplasia* **2001**, *6* (3), 355–64.

(18) Joshi, S.; Kumar, S.; Choudhury, A.; Ponnusamy, M. P.; Batra, S. K. Altered Mucins (MUC) Trafficking in Benign and Malignant Conditions. *Oncotarget* **2014**, *5* (17), 7272–84.

(19) Duraisamy, S.; Kufe, T.; Ramasamy, S.; Kufe, D. Evolution of the human MUC1 oncoprotein. *Int. J. Oncol.* **2007**, *31* (3), 671–7.

(20) Rahn, J. J.; Dabbagh, L.; Pasdar, M.; Hugh, J. C. The importance of MUC1 cellular localization in patients with breast carcinoma: an immunohistologic study of 71 patients and review of the literature. *Cancer* **2001**, *91* (11), 1973–82.

(21) Cheung, K. L.; Graves, C. R.; Robertson, J. F. Tumour marker measurements in the diagnosis and monitoring of breast cancer. *Cancer Treat. Rev.* **2000**, *26* (2), 91–102.

(22) Kufe, D. W. Mucins in cancer: function, prognosis and therapy. *Nat. Rev. Cancer* **2009**, *9* (12), 874–85.

(23) Kagaya, H.; Oba, M.; Miura, Y.; Koyama, H.; Ishii, T.; Shimada, T.; Takato, T.; Kataoka, K.; Miyata, T. Impact of polyplex micelles installed with cyclic RGD peptide as ligand on gene delivery to vascular lesions. *Gene Ther.* **2012**, *19* (1), 61–9.

(24) Levy-Nissenbaum, E.; Radovic-Moreno, A. F.; Wang, A. Z.; Langer, R.; Farokhzad, O. C. Nanotechnology and aptamers: applications in drug delivery. *Trends Biotechnol.* **2008**, *26* (8), 442–9.

(25) Ellington, A. D.; Szostak, J. W. In vitro selection of RNA molecules that bind specific ligands. *Nature* **1990**, *346* (6287), 818–22.

(26) Tavitian, B. In vivo imaging with oligonucleotides for diagnosis and drug development. *Gut* **2003**, *52* (Suppl 4), iv40–7.

(27) Pieve, C. D.; Perkins, A. C.; Missailidis, S. Anti-MUC1 aptamers: radiolabelling with (99m)Tc and biodistribution in MCF-7 tumour-bearing mice. *Nucl. Med. Biol.* **2009**, *36* (6), 703–10.

(28) Borbas, K. E.; Ferreira, C. S. M.; Perkins, A.; Bruce, J. I.; Missailidis, S. Design and Synthesis of Mono- and Multimeric Targeted Radiopharmaceuticals Based on Novel Cyclen Ligands Coupled to Anti-MUC1 Aptamers for the Diagnostic Imaging and Targeted Radiotherapy of Cancer. *Bioconjugate Chem.* **2007**, *18* (4), 1205–1212.

(29) Ferreira, C. S.; Cheung, M. C.; Missailidis, S.; Bisland, S.; Gariepy, J. Phototoxic aptamers selectively enter and kill epithelial cancer cells. *Nucleic Acids Res.* **2009**, *37* (3), 866–76.

(30) Kurosaki, T.; Higuchi, N.; Kawakami, S.; Higuchi, Y.; Nakamura, T.; Kitahara, T.; Hashida, M.; Sasaki, H. Self-assemble gene delivery system for molecular targeting using nucleic acid aptamer. *Gene* **2012**, *491* (2), 205–209.

(31) Yin, H.; Kanasty, R. L.; Eltoukhy, A. A.; Vegas, A. J.; Dorkin, J. R.; Anderson, D. G. Non-viral vectors for gene-based therapy. *Nat. Rev. Genet.* **2014**, *15* (8), 541–55.

(32) Midoux, P.; Pichon, C.; Yaouanc, J. J.; Jaffres, P. A. Chemical vectors for gene delivery: a current review on polymers, peptides and lipids containing histidine or imidazole as nucleic acids carriers. *Br. J. Pharmacol.* **2009**, *157* (2), 166–78.

(33) Al-Dosari, M. S.; Gao, X. Nonviral gene delivery: principle, limitations, and recent progress. *AAPS J.* **2009**, *11* (4), 671–81.

(34) Konstan, M. W.; Davis, P. B.; Wagener, J. S.; Hilliard, K. A.; Stern, R. C.; Milgram, L. J.; Kowalczyk, T. H.; Hyatt, S. L.; Fink, T. L.; Gedeon, C. R.; Oette, S. M.; Payne, J. M.; Muhammad, O.; Ziady, A. G.; Moen, R. C.; Cooper, M. J. Compacted DNA nanoparticles administered to the nasal mucosa of cystic fibrosis subjects are safe and demonstrate partial to complete cystic fibrosis transmembrane regulator reconstitution. *Hum. Gene Ther.* **2004**, *15* (12), 1255–69.

(35) Ramamoorth, M.; Narvekar, A. Non viral vectors in gene therapy- an overview. *J. Clin Diagn Res.* **2015**, *9* (1), GE01–6.

(36) Gao, X.; Kim, K. S.; Liu, D. Nonviral gene delivery: what we know and what is next. *AAPS J.* **2007**, *9* (1), E92–104.

(37) Swami, A.; Goyal, R.; Tripathi, S. K.; Singh, N.; Katiyar, N.; Mishra, A. K.; Gupta, K. C. Effect of homobifunctional crosslinkers on nucleic acids delivery ability of PEI nanoparticles. *Int. J. Pharm.* **2009**, *374* (1–2), 125–38.

(38) Fischer, D.; Bieber, T.; Li, Y.; Elsasser, H. P.; Kissel, T. A novel non-viral vector for DNA delivery based on low molecular weight, branched polyethylenimine: effect of molecular weight on transfection efficiency and cytotoxicity. *Pharm. Res.* **1999**, *16* (8), 1273–9.

(39) Arias, F. J.; Santos, M.; Fernandez-Colino, A.; Pinedo, G.; Girotti, A. Recent contributions of elastin-like recombinamers to biomedicine and nanotechnology. *Curr. Top. Med. Chem.* **2014**, *14* (6), 819–36.

(40) Garcia-Arevalo, C.; Bermejo-Martin, J. F.; Rico, L.; Iglesias, V.; Martin, L.; Rodriguez-Cabello, J. C.; Arias, F. J. Immunomodulatory nanoparticles from elastin-like recombinamers: single-molecules for tuberculosis vaccine development. *Mol. Pharmaceutics* **2013**, *10* (2), 586–97.

(41) de Torre, I. G.; Wolf, F.; Santos, M.; Rongen, L.; Alonso, M.; Jockenhoevel, S.; Rodríguez-Cabello, J. C.; Mela, P. Elastin-like recombinamer-covered stents: Towards a fully biocompatible and

non-thrombogenic device for cardiovascular diseases. *Acta Biomater.* **2015**, *12* (0), 146.

(42) McDaniel, J. R.; Macewan, S. R.; Dewhirst, M.; Chilkoti, A. Doxorubicin-conjugated chimeric polypeptide nanoparticles that respond to mild hyperthermia. *J. Controlled Release* **2012**, *159* (3), 362−7.

(43) Rodriguez-Cabello, J. C.; Piña, M. J.; Ibáñez-Fonseca, A.; Fernandez-Colino, A.; Arias, F. J. Nanotechnological approach to the therapeutic delivery using elastin-like recombinamers. *Bioconjugate Chem.* **2015**, *26*, 1252.

(44) Urry, D. W. *What Sustains Life? Consilient Mechanisms for Protein-Based Machines and Materials*; Springer-Verlag: New York, 2006.

(45) Chen, T. H.; Bae, Y.; Furgeson, D. Y. Intelligent biosynthetic nanobiomaterials (IBNs) for hyperthermic gene delivery. *Pharm. Res.* **2008**, *25* (3), 683−91.

(46) Piña, M. J.; Alex, S. M.; Arias, F. J.; Santos, M.; Rodriguez-Cabello, J. C.; Ramesan, R. M.; Sharma, C. P. Elastin-like recombinamers with acquired functionalities for gene-delivery applications. *J. Biomed. Mater. Res., Part A* **2015**, *103*, 3166.

(47) Shen, W.; van Dongen, M. A.; Han, Y.; Yu, M.; Li, Y.; Liu, G.; Banaszak Holl, M. M.; Qi, R. The role of caveolin-1 and syndecan-4 in the internalization of PEGylated PAMAM dendrimer polyplexes into myoblast and hepatic cells. *Eur. J. Pharm. Biopharm.* **2014**, *88*, 658.

(48) Blau, S.; Jubeh, T. T.; Haupt, S. M.; Rubinstein, A. Drug targeting by surface cationization. *Crit. Rev. Ther. Drug Carrier Syst.* **2000**, *17* (5), 425−65.

(49) Mintzer, M. A.; Simanek, E. E. Nonviral vectors for gene delivery. *Chem. Rev.* **2009**, *109* (2), 259−302.

(50) Poyet, J.-L.; Hoeveler, A. cDNA cloning and expression of pokeweed antiviral protein from seeds in Escherichia coli and its inhibition of protein synthesis in vitro. *FEBS Lett.* **1997**, *406* (1−2), 97−100.

(51) Rodriguez-Cabello, J. C.; Girotti, A.; Ribeiro, A.; Arias, F. J. Synthesis of genetically engineered protein polymers (recombinamers) as an example of advanced self-assembled smart materials. *Methods Mol. Biol.* **2012**, *811*, 17−38.

(52) Sallach, R. E.; Cui, W.; Balderrama, F.; Martinez, A. W.; Wen, J.; Haller, C. A.; Taylor, J. V.; Wright, E. R.; Long, R. C., Jr; Chaikof, E. L. Long-term biostability of self-assembling protein polymers in the absence of covalent crosslinking. *Biomaterials* **2010**, *31* (4), 779−791.

(53) Butash, K. A.; Natarajan, P.; Young, A.; Fox, D. K. Reexamination of the effect of endotoxin on cell proliferation and transfection efficiency. *Biotechniques* **2000**, *29* (3), 610−4 616, 618−9..

(54) Pinedo-Martín, G.; Castro, E.; Martín, L.; Alonso, M.; Rodríguez-Cabello, J. C. Effect of Surfactants on the Self-Assembly of a Model Elastin-like Block Corecombinamer: From Micelles to an Aqueous Two-Phase System. *Langmuir* **2014**, *30* (12), 3432−3440.

(55) Ren, L.; Marquardt, M. A.; Lech, J. J. Estrogenic effects of nonylphenol on pS2, ER and MUC1 gene expression in human breast cancer cells-MCF-7. *Chem.-Biol. Interact.* **1997**, *104* (1), 55−64.

(56) Croce, M. V.; Isla-Larrain, M. T.; Capafons, A.; Price, M. R.; Segal-Eiras, A. Humoral immune response induced by the protein core of MUC1 mucin in pregnant and healthy women. *Breast Cancer Res. Treat.* **2001**, *69* (1), 1−11.

(57) Su, X.; Fricke, J.; Kavanagh, D. G.; Irvine, D. J. In Vitro and in Vivo mRNA Delivery Using Lipid-Enveloped pH-Responsive Polymer Nanoparticles. *Mol. Pharmaceutics* **2011**, *8* (3), 774−787.

(58) Xiao, Z.; Levy-Nissenbaum, E.; Alexis, F.; Lupták, A.; Teply, B. A.; Chan, J. M.; Shi, J.; Digga, E.; Cheng, J.; Langer, R.; Farokhzad, O. C. Engineering of Targeted Nanoparticles for Cancer Therapy Using Internalizing Aptamers Isolated by Cell-Uptake Selection. *ACS Nano* **2012**, *6* (1), 696−704.

(59) Sahay, G.; Alakhova, D. Y.; Kabanov, A. V. Endocytosis of nanomedicines. *J. Controlled Release* **2010**, *145* (3), 182−95.

(60) Rejman, J.; Oberle, V.; Zuhorn, I. S.; Hoekstra, D. Size-dependent internalization of particles via the pathways of clathrin- and caveolae-mediated endocytosis. *Biochem. J.* **2004**, *377* (1), 159−69.

(61) García-Arévalo, C.; Bermejo-Martín, J. F.; Rico, L.; Iglesias, V.; Martín, L.; Rodríguez-Cabello, J. C.; Arias, F. J. Immunomodulatory Nanoparticles from Elastin-Like Recombinamers: Single-Molecules for Tuberculosis Vaccine Development. *Mol. Pharmaceutics* **2013**, *10* (2), 586−597.

(62) Bessa, P. C.; Machado, R.; Nurnberger, S.; Dopler, D.; Banerjee, A.; Cunha, A. M.; Rodriguez-Cabello, J. C.; Redl, H.; van Griensven, M.; Reis, R. L.; Casal, M. Thermoresponsive self-assembled elastin-based nanoparticles for delivery of BMPs. *J. Controlled Release* **2010**, *142* (3), 312−8.

(63) Sarangthem, V.; Cho, E. A.; Bae, S. M.; Singh, T. D.; Kim, S. J.; Kim, S.; Jeon, W. B.; Lee, B. H.; Park, R. W. Construction and Application of Elastin Like Polypeptide Containing IL-4 Receptor Targeting Peptide. *PLoS One* **2013**, *8* (12), e81891.

(64) Dash, B. C.; Mahor, S.; Carroll, O.; Mathew, A.; Wang, W. X.; Woodhouse, K. A.; Pandit, A. Tunable elastin-like polypeptide hollow sphere as a high payload and controlled delivery gene depot. *J. Controlled Release* **2011**, *152* (3), 382−392.

(65) Costa, R. R.; Girotti, A.; Santos, M.; Arias, F. J.; Mano, J. F.; Rodriguez-Cabello, J. C. Cellular uptake of multilayered capsules produced with natural and genetically engineered biomimetic macromolecules. *Acta Biomater.* **2014**, *10* (6), 2653−62.

(66) Hunter, A. C. Molecular hurdles in polyfectin design and mechanistic background to polycation induced cytotoxicity. *Adv. Drug Delivery Rev.* **2006**, *58* (14), 1523−1531.

(67) Fischer, D.; Bieber, T.; Li, Y.; Elsässer, H.-P.; Kissel, T. A Novel Non-Viral Vector for DNA Delivery Based on Low Molecular Weight, Branched Polyethylenimine: Effect of Molecular Weight on Transfection Efficiency and Cytotoxicity. *Pharm. Res.* **1999**, *16* (8), 1273−1279.

(68) Deng, R.; Yue, Y.; Jin, F.; Chen, Y.; Kung, H. F.; Lin, M. C.; Wu, C. Revisit the complexation of PEI and DNA - how to make low cytotoxic and highly efficient PEI gene transfection non-viral vectors with a controllable chain length and structure? *J. Controlled Release* **2009**, *140* (1), 40−6.

(69) Sajeesh, S.; Choe, J. Y.; Lee, T. Y.; Lee, D.-k. Guanidine modified polyethyleneimine-g-polyethylene glycol nanocarriers for long interfering RNA (liRNA) based advanced anticancer therapy. *J. Mater. Chem. B* **2015**, *3* (2), 207−216.

(70) Kievit, F. M.; Veiseh, O.; Bhattarai, N.; Fang, C.; Gunn, J. W.; Lee, D.; Ellenbogen, R. G.; Olson, J. M.; Zhang, M. PEI−PEG−Chitosan-Copolymer-Coated Iron Oxide Nanoparticles for Safe Gene Delivery: Synthesis, Complexation, and Transfection. *Adv. Funct. Mater.* **2009**, *19* (14), 2244−2251.

(71) Yu, C.; Hu, Y.; Duan, J.; Yuan, W.; Wang, C.; Xu, H.; Yang, X. D. Novel aptamer-nanoparticle bioconjugates enhances delivery of anticancer drug to MUC1-positive cancer cells in vitro. *PLoS One* **2011**, *6* (9), e24077.

(72) Hsu, C. Y.; Uludag, H. A simple and rapid nonviral approach to efficiently transfect primary tissue-derived cells using polyethylenimine. *Nat. Protoc.* **2012**, *7* (5), 935−45.

(73) Kumar, P.; Lindberg, L.; Thirkill, T. L.; Ji, J. W.; Martsching, L.; Douglas, G. C. The MUC1 Extracellular Domain Subunit Is Found in Nuclear Speckles and Associates with Spliceosomes. *PLoS One* **2012**, *7* (8), e42712.

(74) Kufe, D. W. MUC1-C oncoprotein as a target in breast cancer: activation of signaling pathways and therapeutic approaches. *Oncogene* **2013**, *32* (9), 1073−81.

(75) Shapira, A.; Benhar, I. Toxin-based therapeutic approaches. *Toxins* **2010**, *2* (11), 2519−83.

(76) Orimo, A.; Gupta, P. B.; Sgroi, D. C.; Arenzana-Seisdedos, F.; Delaunay, T.; Naeem, R.; Carey, V. J.; Richardson, A. L.; Weinberg, R. A. Stromal fibroblasts present in invasive human breast carcinomas promote tumor growth and angiogenesis through elevated SDF-1/CXCL12 secretion. *Cell* **2005**, *121* (3), 335−48.

(77) Ling, X.; Marini, F.; Konopleva, M.; Schober, W.; Shi, Y.; Burks, J.; Clise-Dwyer, K.; Wang, R. Y.; Zhang, W.; Yuan, X.; Lu, H.; Caldwell, L.; Andreeff, M. Mesenchymal Stem Cells Overexpressing IFN-beta Inhibit Breast Cancer Growth and Metastases through Stat3

1284 Signaling in a Syngeneic Tumor Model. *Cancer Microenviron.* **2010**, *3*
1285 (1), 83−95.